Two-Dimensional Penning Ionization Electron Spectroscopy of CH_2ClI and CH_2ClCN

Shan Xi Tian, Naoki Kishimoto, and Koichi Ohno*

Department of Chemistry, Graduate School of Science, Tohoku University, Aramaki, Aoba-ku, Sendai 980-8578, Japan

Received: September 6, 2002; In Final Form: November 11, 2002

The electronic structures of CH_2ClI and CH_2ClCN and anisotropic interactions with the metastable He*(2^3S) atoms are studied by two-dimensional (electron-energy and collision-energy-resolved) Penning ionization electron spectroscopy as well as He I ultraviolet photoelectron spectroscopy. A broad band with the high ionization potentials in the Penning ionization electron spectrum of CH_2ClI is proposed to be related to autoionizations of the Cl** or I** species produced through dissociations after the excitation transfer from the He* atom. The split bands having the characteristics of the Cl and I lone pair electrons (n_{Cl} and n_I) are observed in the spectra, as being interpreted by the intramolecular orbital ($n_{Cl} \leftrightarrow n_I$ and $n_{Cl} \leftrightarrow \pi_{CN}$) through-space/through-bond interactions rather than the spin−orbit coupling effects. The magnitude of intramolecular orbital $n_{Cl} \leftrightarrow \pi_{CN}$ interactions is much stronger than that of the $n_{Cl} \leftrightarrow n_I$ interactions. The collision energy dependence of partial Penning ionization cross sections is interpreted on the basis of the delocalized characteristics of the electron distributions for respective molecular orbitals and the model calculations of the interaction potential energies.

I. Introduction

In a chemiionization process known as Penning ionization ($A^* + M \rightarrow M^+ + A + e^-$), a target molecule (or atom) M is ionized by collision with a metastable atom A* having an excitation energy larger than the lowest ionization potential (IP) of the molecule.[1] The total ionization cross sections σ_T for various atoms and molecules with He*(2^3S) metastable atoms are extensively studied by crossed-beam experiments and flowing afterglow.[2−9] One of the most meaningful aspects of the ionization cross sections is their dependence on the relative kinetic energy (i.e., collision energy, E_c). Illenberger and Niehaus have found that the $\sigma_T(E_c)$ for an atomic target is mainly governed by the radial distance dependence of the entrance covalent potential and the transition rate.[2,10] Because the excitation energy of He*(2^3S), 19.820 eV, is larger than some IPs of molecular orbitals (MO), there are usually several final electronic states that can be produced in the Penning ionizations. The partial ionization cross sections for different ionic states $\sigma(E_c)$, unlike the $\sigma_T(E_c)$, exhibit distinctly different collision energy dependence if the interaction potentials are anisotropic. This can be interpreted with the electron exchange model[11] and spatial MO density distributions.[12] In the electron exchange model, an MO electron of the target M is transferred to the inner-shell orbital of A* and the excited electron of A* is ejected as Penning electron e^-. For an MO, its electrons are more or less localized on a particular part of the molecule. Thereby, preferential orientations for the transition may differ for different ionic states, reflecting the anisotropy of interactions. Moreover, other interaction potentials may have influence on the $\sigma(E_c)$, i.e., avoided surface crossing with nonadiabatic transitions to molecular Rydberg (or superexcited) states or the ionic-pair of $He^+ + M^-$.[13−16] For these cases, $\sigma(E_c)$ functions depend not only on the final ionic states but also on these intermediate complexes.[15]

Penning ionization electron spectrum (PIES) can be obtained by analyzing the kinetic energies (E_e) of Penning electrons.[10,13,17] In recent decades, a coupled technique including velocity selection (or collision-energy-resolved) and electron energy analysis has been developed.[18−24] It is noted that a pioneering work of studying the collision-energy-resolved PIES (CERPIES) was done by Hotop through changing temperature of the metastable beam for atomic targets about 30 years ago.[25] In our laboratory, we use the pseudorandom modulating cross-correlation time-of-flight (TOF) method[26,27] to improve the detecting efficiency, and collision energy dependence of the partial cross sections (CEDPICS) can be measured simultaneously. Thereby, two-dimensional (electron-energy and collision-energy-resolved) PIES (2D-PIES) can be obtained efficiently.[24] Furthermore, slope parameters (m) are available by a least-squares fitting of the plots of CEDPICS against the E_c values for an ionic state or ionization band. We can get information of anisotropic interactions of the steric access of A* to M. Typically, a negative m value accompanied by a negative peak shift (ΔE) shows that there is an attractive region for a certain MO; a positive m value accompanied by a positive ΔE shows a repulsive case. Here the peak shift ΔE is the difference of E_e for a specific band in the PIES with respect to that in the He I ultraviolet photoelectron spectrum (UPS), namely, it can be obtained as the differences between the peak positions in PIES (E_{PIES}, in electron energy scale) and the nominal value (E_0, difference between the metastable excitation energy and sample IP), $\Delta E = E_{PIES} - E_0$. For a PIES of a molecular target collided by a metastable noble gas atom, the value of ΔE for a specific orbital is approximated to be equal to the well depth of the calculated interaction potential for the specific direction in the entrance channel.[28]

Recently, nonbonding lone pair orbitals (n_X) of halogen atoms (X= F, Cl, Br, and I) attracted our interest because the n_X orbitals usually play an important role (as electron donor) in hydrogen bonding and the arguments of the relationship between

* To whom correspondence should be addressed.

10.1021/jp021986x CCC: $25.00
Published on Web 01/01/2003

the corresponding spin−orbit split bands and anisotropic interactions around the halogen atom substituted into a low symmetry hydrocarbon.[29−31] In particular, the slope parameters *m* are almost equal for the split bands mainly arising from spin−orbit coupling effects.[30,31] However, when intramolecular orbital through-bond or through-space interactions are stronger than the spin−orbit coupling effect, the contributions from the other molecular parts together with the lone pair electrons of the halogen atom are the compositions of an MO. This can be reflected by the band shapes and intensities and CEDPICS which distinctly differ from those of the pure n_X bands.[31] Novak and co-workers reported a series of studies on halogen−halogen ($n_X \leftrightarrow n_X$) interactions in halogenomethanes because it allows accurate determination of the intramolecular orbital interactions between the germinal halogens.[32−34] Moreover, the halogen species can be produced by photoexcitation followed by dissociations of halogenomethanes, so these molecules can play the crucial roles in atmospheric chemistry (ozone layer and greenhouse effects).[35]

Molecular CH_2BrCl,[32] $CHBrCl_2$,[33] and CH_2ClI[32] have been investigated by Novak et al. using He I and He II photoelectron spectroscopy and angle-resolved photoelectron spectroscopy with the synchrotron radiation. They found that the intramolecular orbital interactions in the latter two molecules are stronger than those in the first one. More recently, we also found that the orbital interactions in CH_2BrCl are much weaker with respect to the interactions in $CHBrCl_2$, by the 2D-PIES studies.[31] However, these conclusions for CH_2BrCl and CH_2ClI are inconsistent with those derived recently by Novak et al. in which the $n_{Cl} \leftrightarrow n_I$ interaction (0.34 ∼ 0.50 eV) is much weaker than the $n_{Cl} \leftrightarrow n_{Br}$ interaction (0.43∼1.53 eV).[34] It is worth obtaining insights into the intramolecular orbital interactions, especially using the 2D-PIES technique. As mentioned above, if the intramolecular orbital interactions are relatively weak, the split bands for halogen atoms are mainly arising from the strong spin−orbit coupling effects. Correspondingly, CEDPICS exhibits almost equal *m* values for the spin−orbit split bands, otherwise, it shows the different *m* values for the strong orbital interactions. In this work, CH_2ClI and CH_2ClCN are selected for the investigations on the $n_{Cl} \leftrightarrow n_{Br}$ and $n_{Cl} \leftrightarrow \pi_{CN}$ orbital interactions.

II. Experimental Method

Details of the experimental apparatus have been reported elsewhere.[18−20] Metastable atoms of He*(2^1S, 2^3S) were produced by a discharged nozzle source with a tantalum hollow cathode. The He*(2^1S) component was quenched by a water-cooled helium discharge lamp. He I resonance photons (584 Å, 21.22 eV) produced by a discharge in pure helium gas were used to obtain UPS. The kinetic energies of the electrons ejected in Penning ionization or photoionization were determined by a hemispherical electrostatic deflection type analyzer using an electron collection angle 90° to the incident He*(2^3S) beam axis or He I light beam axis. The energy resolution of the electron analyzer was estimated to be 80 meV from the full width at half-maximum (fwhm) of the $Ar^+(^2P_{3/2})$ peak in the He I UPS for the energy-higher-resolution PIES and UPS measurements of the samples; for the CEDPICS measurements, the resolution was lowered to 250 meV in order to obtain higher electron counting rates. The transmission efficiency curves of the electron energy analyzer for both of these two modes were determined by comparing our UPS data of some molecules with those obtained by Gardner and Samson[36] and Kimura et al.[37] The calibration of the electron energy scale was made with reference to the lowest ionic state of molecule nitrogen mixed with the sample molecule in He I UPS ($E_e = 5.639$ eV)[38] and He*(2^3S) PIES ($E_e = 4.292$ eV)[39] including a peak energy shift of 50 meV and the difference between the metastable excitation energy and the lowest ionization potential (IP).

For the collision-energy-resolved measurements of Penning ionization, the metastable He*(2^3S) beam was modulated by a pseudorandom chopper rotating at ca. 400 Hz and then introduced into a reaction cell located at 504 mm downstream from the chopper disk. Time dependent electron signals for each kinetic electron energy E_e were recorded with scanning electron energies of a 40 meV step, and the dwell time for the TOF measurements was 3μs. The two-dimensional data as functions of E_e and time *t* were stored in a 2MB RAM. Two-dimensional spectra $I_e(E_e,t_{TOF})$, functions of E_e and TOF, can lead to $I_e(E_e,v_{He^*})$, functions of E_e and the velocity of He* (v_{He^*}), and then to the two-dimensional Penning ionization cross-section $\sigma(E_e,v_r)$ using the equations

$$\sigma(E_e,v_r) = c[I_e(E_e,v_{He^*})/I_{He^*}(v_{He^*})](v_{He^*}/v_r) \quad (1)$$

$$v_r = [v_{He^*}{}^2 + (3kT/M)]^{1/2} \quad (2)$$

where *c* is a constant, v_r is the relative velocity averaged over the velocity of the target molecule, *k* is the Boltzmann constant, and *T* and *M* are the gas temperature and mass of target molecule, respectively. The velocity distribution $I_{He^*}(v_{He^*})$ of the He* beam was determined by monitoring secondary electrons emitted from the inserted stainless steel plate. Finally, $\sigma(E_e,v_r)$ was normalized by $I_{He^*}(v_{He^*})$ and converted to $\sigma(E_e,E_c)$, functions of E_e and E_c, using the relation

$$E_c = \mu v_r{}^2/2 \quad (3)$$

where μ is the reduced mass of the system. The CEDPICS were obtained from $\sigma(E_e,E_c)$ data within an appropriate range of E_e (typically the fwhm of the respective band) to avoid the effect of neighboring bands. The CERPIES were cut at the two E_c (∼100 and ∼250 meV) values from $\sigma(E_e,E_c)$ data with some width.

The high purity samples CH_2ClI and CH_2ClCN were purchased from Wako Pure Chemical Industries Ltd., and they were used after several freeze−pump−thawed cycles. The liquid sample was contained in a Pyrex tube out of the chamber in the experiments, and the Pyrex tube was connected with a steel tube inserted into the reaction cell in the chamber. The volatility of the samples at room temperature was high enough to create a sufficient concentration of target molecules in the gas phase, the ambient pressure was controlled at ca. 2×10^{-5} Torr.

III. Calculation

The geometrical parameters of CH_2ClI and CH_2ClCN at C_s symmetry were optimized at the second-order Møller−Plesset perturbation (MP2) method with the 6-311+G(d,p) and the Stephens-Basch-Krauss ECP split valence basis set[40] augmented with a d polarization function [ECP-31G(d)] for I atom. In the electron density contour maps obtained by Hartree−Fock self-consistent-field (HF−SCF) calculations with the 6-311+G(d,p) and ECP-31G(d) basis sets, thick solid curves indicate the repulsive molecular surface approximated by atomic spheres of van der Waals radii ($r_C = 1.7$ Å, $r_H = 1.2$ Å, $r_{Cl} = 1.8$ Å, $r_N = 1.5$ Å, $r_I = 2.15$ Å).[41] The IP values for each molecule were predicted with the outer-valence Green's function (OVGF)[42] method with the 6-31+G(d,p) and ECP-31G(d) basis sets.

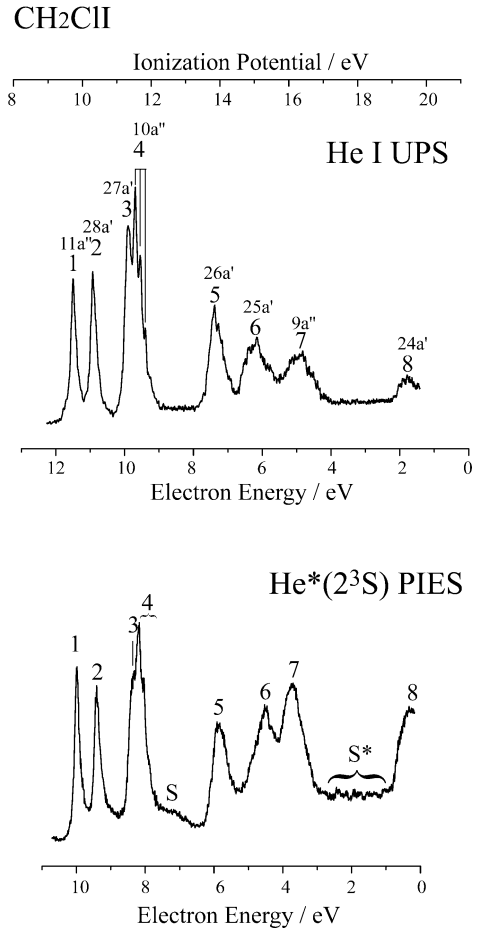

Figure 1. He I UPS and He*(2^3S) PIES of CH_2ClI.

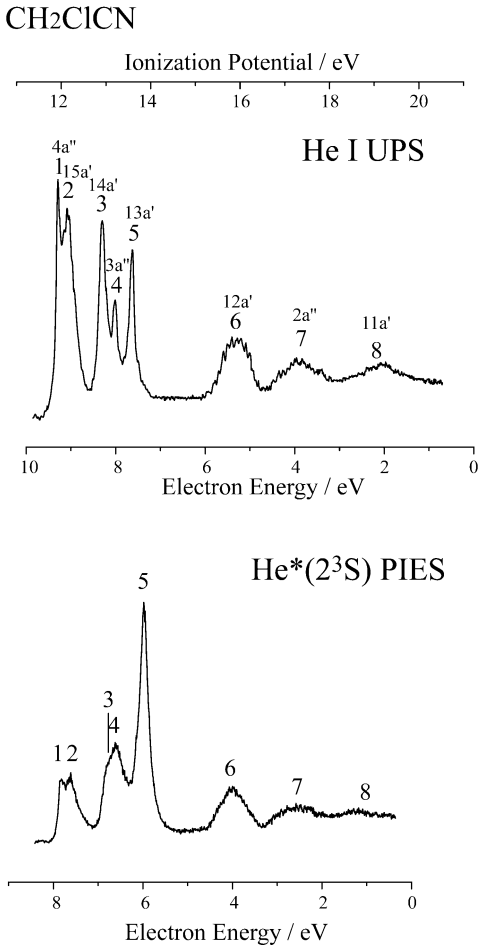

Figure 2. He I UPS and He*(2^3S) PIES of CH_2ClCN.

It is well-known that the shape of velocity dependence of the total scattering cross section of He*(2^3S) by He, Ar, and Kr is very similar to that of Li(2^2S),[43] and interaction well depths and the location of potential wells have been found to be very similar for interactions of various targets with He*(2^3S) and Li(2^2S).[2,3,17,25,44,45] So, this similarity between He*(2^3S) and Li(2^2S) is usually used to compare the computationally much more feasible Li−M potentials with the experimental results on the He*(2^3S)−M interactions.[15,27,29−31] In this work, the interaction potential calculations with the Li(2^2S) atom, $V^*(R,\theta)$ (where R and θ are defined in the captions), were performed at the unrestricted MP2 level of theory using the 6-31+G(d,p) and ECP-31G(d) basis sets with scanning R or θ values and the geometrical parameters of the targets fixed at the previously optimized values. Spin-contamination is negligible for these calculations. The present calculations of interaction potentials and IP values were performed with Gaussian 98.[46]

IV. Results and Discussion

A. Results. Figures 1 and 2 show the He I UPS and He*-(2^3S) PIES of CH_2ClI and CH_2ClCN, respectively. The electron energy scales for PIES are shifted 1.40 eV relative to those for UPS by the difference in the excitation energies between the He I photon (21.22 eV) and the He*(2^3S) atom (19.82 eV). The orbitals for the assignments in the spectra of CH_2ClI have been numbered from the core orbital, which differs from those given by Novak et al.[32]

The CERPIES obtained from 2D-PIES of CH_2ClI and CH_2ClCN are shown in Figures 3 and 4, respectively. Hot spectra ($E_c \sim 250$ meV) are represented by the broken curves; cold spectra ($E_c \sim 100$ meV) are represented by the solid curves.

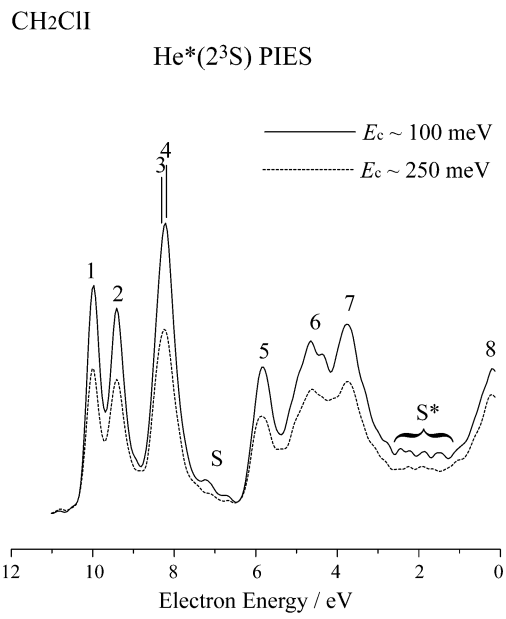

Figure 3. Collision-energy-resolved He*(2^3S) PIES of CH_2ClI: solid curve, $E_c \sim 98-102$ meV, average 100 meV; dotted curve, $E_c \sim 241-259$ meV, average 250 meV.

The CEDPICS plots against E_c values in the range of 90∼300 meV, log σ vs log E_c, are presented in Figures 5 and 6 for CH_2ClI and CH_2ClCN, respectively. The calculated electron density maps plotted on the molecular nodal planes (for a″-type orbitals, the plane at the distance 1.7 Å above the nodal plane) are shown

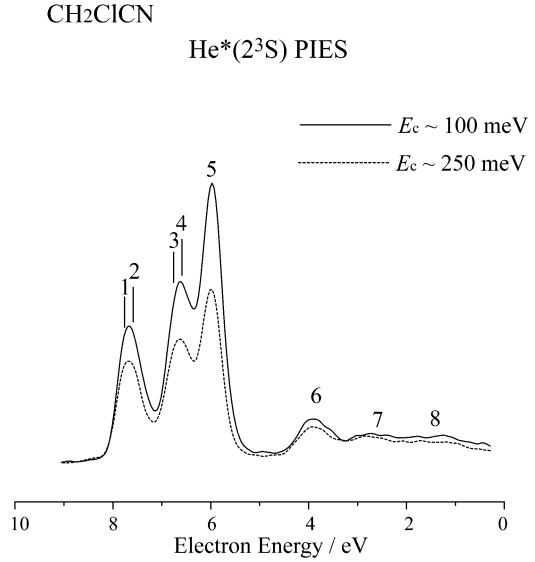

Figure 4. Collision-energy-resolved He*(2^3S) PIES of CH_2ClCN: solid curve, $E_c \sim 98-102$ meV, average 100 meV; dotted curve, $E_c \sim 242-258$ meV, average 250 meV.

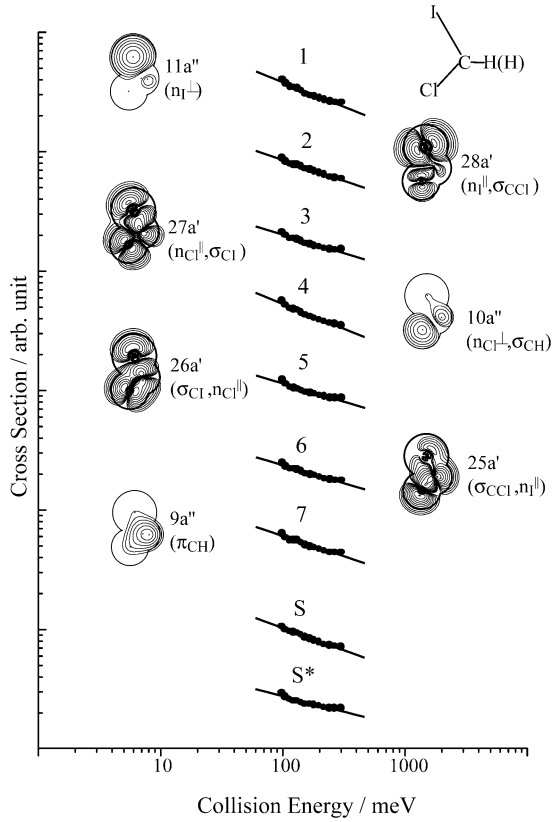

Figure 5. Collision energy dependence of partial ionization cross sections for CH_2ClI collided by He*(2^3S). Electron density maps of the a″-type orbitals are plotted on a plane above 1.7 Å from the nodal plane.

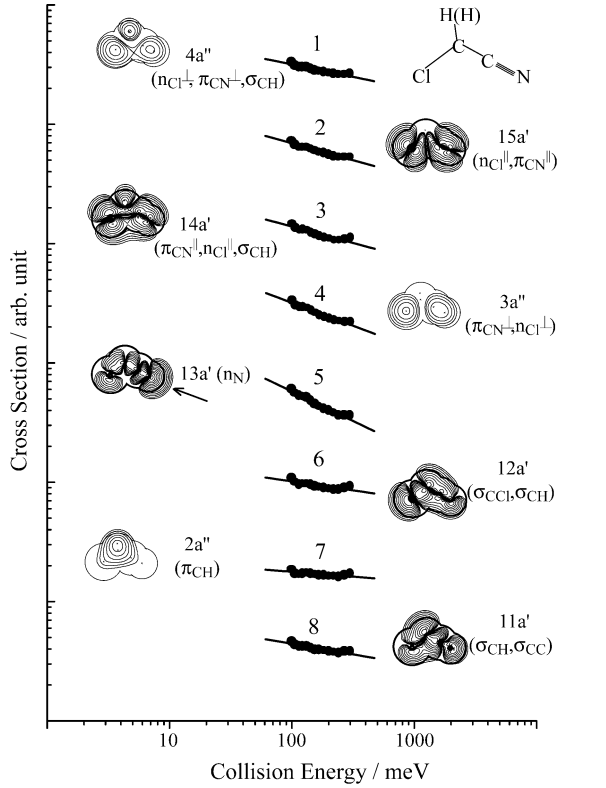

Figure 6. Collision energy dependence of partial ionization cross sections for CH_2ClCN collided by He*(2^3S). Electron density maps of the a″-type orbitals are plotted on a plane above 1.7 Å from the nodal plane.

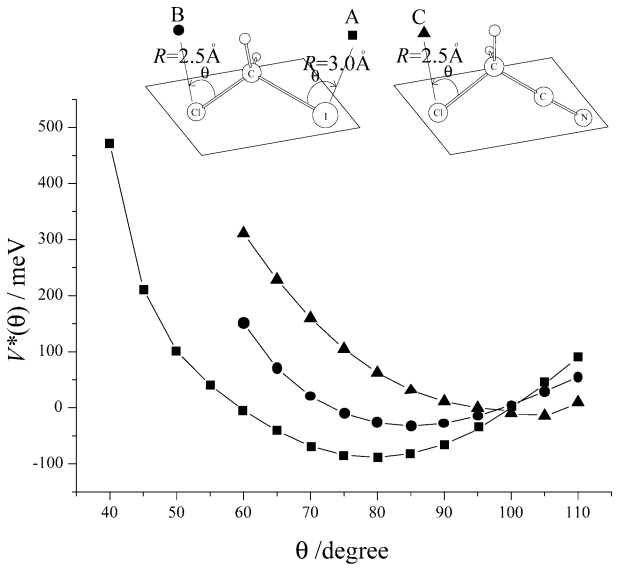

Figure 7. Interaction potential energy curves $V^*(\theta)$ by scanning θ values on the molecular nodal plane: A (■) is scanning θ value around the I in CH_2ClI; B (●) is scanning θ value around the Cl in CH_2ClI; C (▲) is scanning θ value around the Cl in CH_2ClCN. The distances between the Li and Cl or I atoms are shown in the figure.

in order to grasp most effective directions of the ionization or effective access direction of the He* atom.

For the studies of the intramolecular orbital interactions, the interaction potential curves $V^*(\theta)$ around the Cl and I atoms are shown in Figure 7. The interaction potential curves $V^*(R)$ for the approaches to the Cl, I, C atoms and the CN bond are shown in Figure 8.

Tables 1 and 2 summarize the band assignments with orbital characteristics, the calculated and observed (in the He I UPS of this work) IP values, the peak shifts ΔE, and the slope parameters m for each band.

B. He I UPS and He*(2^3S) PIES. The higher energy-resolution (fwhm ~ 15 meV) He I UPS was recorded by Novak et al. for CH_2ClI.[32] Although the vibrational structures assigned to the C−Cl stretching mode cannot be resolved for bands 1 and 2 of the present He I UPS in Figure 1 due to the low energy-resolution (fwhm ~ 80 meV), band 4 of the present He I UPS shows the vibrational structures similar to the previous observa-

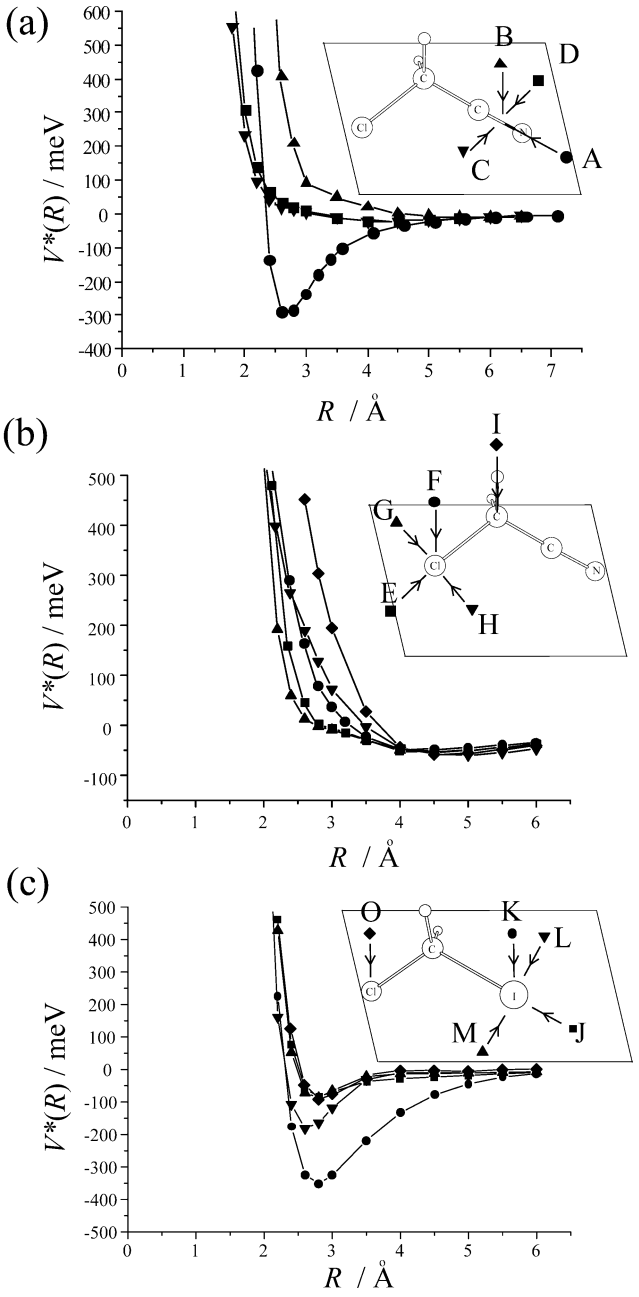

Figure 8. Interaction potential energy curves $V^*(R)$: (a) in the A direction, the He* access is head-on to the N atom and along the CN bond axis; in the B direction, the out-of-plane access is perpendicular to the center of CN bond; in the C and D directions, the in-plane access is perpendicular to the center of CN bond. *R* is the distance between the center of CN bond and the Li atom. (b) The access in the E direction is along the CCl bond axis; the F, G, and H directions represent the approaches perpendicular to the Cl atom; the access to the C atom in the direction I is perpendicular to the molecular nodal plane. (c) The access in the J direction is along the CI bond axis, the in-plane approaches (in the L and M directions) and the out-of-plane access in the K direction are perpendicular to the CI bond axis. The out-of-plane access in the O direction is perpendicular to the CCl bond axis. *R* is the distance between the Cl (in parts b and c) or I (in part c) and Li atoms.

tions.[32] The energy spacing between two sharp peaks of band 4 (see the UPS in Figure 1) is ca. 140 or 150 meV which is close to the vibrational energy of 1392 cm^{-1} (ca. 170 meV) for a free CH_2 scissoring mode. These band structures are closely related to the corresponding orbital compositions. In Figure 5, the density maps for 28a′, 27a′, and 10a″ show the small compositions of σ_{CCl}, σ_{CI}, and σ_{CH} bonds, respectively. There are much fewer σ_{CH} composition for 11a″ with respect to that for 28a′, which is consistent in the observation of the narrower band 1 in the higher energy-resolved UPS.[32]

Unlike the spin−orbit split bands of the I atom for the iodohydrocarbons,[47] bands 1 and 2 exhibit the comparable intensities both in the UPS and in the PIES of Figure 1. At the same experimental condition, the n_{Cl} bands for CH_2BrCl are not separated,[31] but bands 3 and 4 for CH_2ClI are resolved clearly in the spectra. Therefore, the band splitting for bands 3 and 4 is owed to the stronger $n_{Cl} \leftrightarrow n_I$ orbital interactions rather than the spin−orbit coupling effects. It is interesting that an additional band is labeled with S in the PIES of Figure 1. Band S cannot be assigned as a shake-up or shake-off satellite band, and the further explanations will be given in section D. This band also seems impossible to be interpreted by the ionic-pair intermediate formation $He^+-Cl^-CH_2I$, because the band related to the ionic-pair intermediate usually shows an extremely large negative slope.[15] Because band S is clearly different from the normal Franck−Condon vibrational distribution for band 4, it may be related to the formation of a superexcited state of CH_2-ClI energetically close to the excitation energy of the $He^*(2^3S)$ atom. Similar bands for specific molecules such as HCl,[48] CO,[49] etc. have been observed in the PIES.

In the PIES of Figure 1, band S* is labeled in the spectral range of IP: 17.13∼18.91 eV, exhibiting some sharp structures superimposed on the underlying broad band. These structures are proposed to be a series of autoionization lines of atomic Cl** or I** which is produced by the excitation transfer, $He^*(2^3S) + CH_2ClI \rightarrow He + CH_2ClI^{**}$, then following with a dissociation, $CH_2ClI^{**} \rightarrow CH_2I + Cl^{**}$ or $CH_2Cl + I^{**}$. The autoionization, Cl^{**} (or I^{**}) $\rightarrow Cl^+$ (or I^+) $+ e^-$, usually corresponds to the sharp electron peaks as well as the underlying broad continuum in the low electron energy region (less than 3 eV).[31,48] Because the atomic structures cannot be well resolved due to the low energy-resolution in this work and there are no theoretical or experimental data on the dissociation energies of CH_2ClI^{**} available in the literatures until now, we cannot give further information on band S*. The excitation-dissociative autoionization of Rydberg state atomic species has been observed in the PIES of CS_2,[15] CH_2BrCl,[31] and HCl.[48]

Moreover, an enhancement of band 8 in the PIES with respect to that in the UPS is observed in Figure 1. This can be interpreted by the formation of an excimer-like state that is partly involved in a C_{2s} type hole in the target molecule which facilitates intramolecular Auger-like autoionization almost selectively from the 24a′ orbital with the C_{2s} character.[20,50] Although 9a″ of CH_2ClI and 2a″ of CH_2ClCN have the MO characteristic π_{CH} (see Figures 5 and 6), the band enhancements in the PIES are significantly different (see Figures 1 and 2). It will be explained by the anisotropic interactions in section D.

If there are no perturbations by the intramolecular interactions to the lone pair electrons of the Cl atom, these electrons should correspond to one overlapped band at the low energy-resolution condition of this work. However, two distinctly separated bands 1 and 2 appear both in the UPS and PIES of Figure 2. Furthermore, it is contrast to the π_{CN} bands in the spectra of CH_2BrCN[31] that two bands 3 and 4 mainly having the π_{CN} characteristic split clearly in the UPS of Figure 2. These can be interpreted by the strong $n_{Cl} \leftrightarrow \pi_{CN}$ interactions. The details will be presented in section C. Moreover, one may notice the great enhancement of band 5 (having the lone pair N electrons of CN group, n_N), which has been observed for the molecules including the CN group.[27,31] Comparing the PIES of CH_2ClI with that of CH_2ClCN, one can find that the background

TABLE 1: Band Assignments, Ionization Potentials (IP, eV), Peak Shifts (ΔE, meV), and Slope Parameters (m) for CH_2ClI

band assignments					
band	orbital character	IP_{obsd}	IP_{OVGF} (pole strength)[a]	ΔE	m
1	$11a''(n_I^{\perp})$	9.72	9.87 (0.95)	−150±10	−0.41
2	$28a'(n_I^{\parallel},\sigma_{CCl})$	10.30	9.88 (0.95)	−100±40	−0.35
3	$27a'(n_{Cl}^{\parallel},\sigma_{CI})$	11.32	10.99 (0.93)	−80±60	−0.31
4	$10a''(n_{Cl}^{\perp},\sigma_{CH})$	11.53[b]	11.42 (0.91)	−190±20[c]	−0.42
5	$26a'(\sigma_{CCl}, n_{Cl}^{\parallel})$	13.85	13.55 (0.91)	−60±60	−0.30
6	$25a'(\sigma_{CCl}, n_I^{\parallel})$	15.12	15.01 (0.90)	−100±80	−0.30
7	$9a''(\pi_{CH})$	16.24	16.37 (0.89)	100±80	−0.34
S		12.17∼13.15[d]			−0.37
S*		17.13∼18.91[d]			−0.26

[a] The OVGF/6-31+G(d,p) calculations over the optimized geometry at the MP2/6-311+G(d,p) level, the split-valence ECP-31G(d) basis set is used for I atom. [b] The IP value of the first vibrational peak of band 4 in the UPS (see Figure 1). The other two are at IP ∼ 11.67 and 11.82 eV. [c] Estimated from for the first vibrational peak of band 4. [d] Obtained from the PIES. See explanations on S and S* bands in text.

TABLE 2: Band Assignments, Ionization Potentials (IP, eV), Peak Shifts (ΔE, meV), and Slope Parameters (m) for CH_2ClCN

band assignments			IP_{OVGF}		
band	orbital character	IP_{obsd}	(pole strength)[a]	ΔE	m
1	$4a''(n_{Cl}^{\perp},\pi_{CN}^{\perp},\sigma_{CH})$	11.93	11.77(0.92)	−80±20	−0.21
2	$15a'(n_{Cl}^{\parallel},\pi_{CN}^{\parallel})$	12.14	11.99(0.91)	−100±40	−0.28
3	$14a'(\pi_{CN}^{\parallel},n_{Cl}^{\parallel},\sigma_{CH})$	12.92	12.40(0.92)	−100±60	−0.27
4	$3a''(\pi_{CN}^{\perp},n_{Cl}^{\perp})$	13.21	12.52(0.91)	−150±20	−0.38
5	$13a'(n_N)$	13.59	13.71(0.89)	−200±10	−0.49
6	$12a'(\sigma_{CCl},\sigma_{CH})$	15.97	15.70(0.91)	20±100	−0.15
7	$2a''(\pi_{CH})$	17.30	17.18(0.91)	40±120	−0.08
8	$11a'(\sigma_{CH},\sigma_{CC},n_N)$	19.17			−0.18

[a] The OVGF/6-31+G(d,p) calculations over the optimized geometry at the MP2/6-311+G(d,p) level.

TABLE 3: Magnitude of Intramolecular Orbital ($n_{Cl} \leftrightarrow n_I$ and $n_{Cl} \leftrightarrow \pi_{CN}$) Interactions and Split Energies of $n_{Cl,I}$ and π_{CN} Orbitals

	reference	energy/meV
	Intramolecular Orbital Interaction[a]	
$n_{Cl} \rightarrow n_I$	CH_3I[b] $\rightarrow CH_2ClI$	160
$n_I \rightarrow n_{Cl}$	CH_3Cl[b] $\rightarrow CH_2ClI$	135
$n_{Cl} \rightarrow \pi_{CN}$	CH_3CN[b] $\rightarrow CH_2ClCN$	855
$\pi_{CN} \rightarrow n_{Cl}$	CH_3Cl[b] $\rightarrow CH_2ClCN$	745
	Split Energy	
n_{Cl}	Cl_2, HCl, etc.[c]	ca. 80[c]
n_I	CH_2ClI	210
π_{CN}	CH_2ClCN	210
	CH_3I, I_2, HI, etc.[b]	560 ∼ 660[b]
	CH_2ClI	580
	CH_2ClCN	290

[a] For $n(\pi)_X \rightarrow n(\pi)_Y$ with a reference $CH_3Y \rightarrow CH_2XY$, the interaction energy = IP [$n(\pi)_Y$, for CH_2XY] − IP [$n(\pi)_Y$, for CH_3Y]. [b] Using the IP values of the n_{Cl}, n_I, and π_{CN} bands from ref 37. [c] The spin−orbit split energies from ref 51.

increases gradually with the decrease of the electron energy (see Figures 1 and 2). In particular, the spectral background for CH_2ClI is relatively high with respect to that for CH_2ClCN in the region of the electron energy less than 3 eV. It suggests that the dissociations as mentioned above should occur preferably for CH_2ClI. Because of the valence ionic states occurring in the low electron energy region, the possible autoionization bands for Cl** species produced by the dissociations of CH_2ClCN** cannot be observed clearly as those in the PIES of CH_2ClI.

C. Intramolecular Orbital Interactions. To elucidate the nature of bands 1, 2, 3, and 4 (in Figures 1 and 2) deferring from the spin−orbit split bands, we need insights into the orbital interactions in these two molecules. Table 3 lists magnitudes of the intramolecular orbital ($n_{Cl} \leftrightarrow n_I$ and $n_{Cl} \leftrightarrow \pi_{CN}$) interactions and split energies of n_{Cl}, n_I, and π_{CN} orbitals observed in the He I UPS. The interaction magnitude was determined by the following calculations in this work: when studying the $n(\pi)_X \rightarrow n(\pi)_Y$ interaction with a reference $CH_3Y \rightarrow CH_2XY$, the magnitude is estimated to be the IP (n or π) differences, IP [$n(\pi)_Y$, for CH_2XY] − IP [$n(\pi)_Y$, for CH_3Y], where the averaged IP (n or π) value is used for the split (n or π) bands observed in the UPS. The split energies arising from the spin−orbit coupling effects[51] or the intramolecular orbital interactions are obtained in the experimental UPS. Because of the interplay of the orbital interactions, the interaction energies exhibit small differences between $n(\pi)_X \rightarrow n(\pi)_Y$ and $n(\pi)_Y \rightarrow n(\pi)_X$. In particular, this difference for the interplay between π_{CN} and n_{Cl} (ca. 110 meV) is much larger than that for the n_{Cl} and n_I (ca. 25 meV). In Table 3, it is easy to find that the $n_{Cl} \leftrightarrow \pi_{CN}$ interactions are significantly stronger than the $n_{Cl} \leftrightarrow n_I$ interactions. The weaker $n_{Cl} \leftrightarrow n_I$ interactions lead to a distinguished split energy (210 meV, much larger than the spin−orbit split energy of ca. 80 meV) of the bands mainly having the n_{Cl} characteristics for CH_2ClI, and this split energy is as large as the value of the bands for CH_2ClCN. However, the split energy of bands (1 and 2 in Figure 1) having the n_I characteristics for CH_2ClI is close to the spin−orbit split value. For CH_2ClCN, two π_{CN} bands split with a large value of 290 meV although the OVGF calculations only predict it to be 80 meV in Table 2. In Table 1, the OVGF calculations also underestimate the split energy between bands 1 and 2 (only 10 meV) in the spectra of Figure 1. Although the OVGF calculations are generally good at predicting the IP value of each band except for these bands, the theories to describe accurately the intramolecular orbital interactions, especially when they compete with the spin−orbit coupling effects, are still waiting for developments.

To review a total effect of the intramolecular orbital interactions, we need to recall the schemes suggested by Rabalais.[52] One is the *before-after* dichotomy of the MOs involved: the magnitude of the interactions can be estimated by calculating the energies of the intramolecular orbital interactions as what we did. For CH_2ClI and CH_2ClCN, the orbital interactions lead to the increase of the IP values for the first bands, namely, the energy levels of the MOs after the interactions become more negative. The other is (further) splitting of the related bands: the energies can be obtained from the experimental spectra (as the split energies given in Table 3). If we summarize these two values for the interactions to a certain part in the molecule, i.e., for the Cl atom in CH_2ClI, the total energy is estimated to be ca. 345 (=135 + 210) meV, whereas it is to be ca. 740 (=160 + 580) meV for the I atom. Similarly, the values are estimated to be ca. 500 and ca. 225 meV for the Cl and Br atoms in CH_2BrCl (obtained from the UPS in our previous work[31]), respec-

tively. The values for the CN group and Cl atom in CH_2ClCN are 1145 and 955 meV, respectively. Generally, the $n_{Cl} \leftrightarrow n_{Br}$ interactions in CH_2BrCl are a little weaker than $n_{Cl} \leftrightarrow n_I$ interactions in CH_2ClI, and the $n_{Cl} \leftrightarrow \pi_{CN}$ interactions in CH_2ClCN are the strongest.

Besides the different magnitudes of the intramolecular orbital interactions, one may find that the electron distribution characteristics of the a′-type orbitals are more complex than those of the a″-type orbitals for these two molecules. This is can be interpreted by the through-space (or through-bond) interactions and energy separations. The a′-type orbitals interact more strongly than the a″-type orbitals because the a′-type orbitals show more complex MO characteristics than the a″-type orbitals. The concepts of through-space and through-bond interactions originally introduced by Hoffmann[53] have been widely used in the discussions of intramolecular orbital interactions.[54,55] For the molecule having two equivalent lone pairs, the symmetrical MO has the lower energy (higher IP), whereas the unsymmetrical MO has the higher energy if the through-space interactions are predominate; the symmetrical MO has the higher energy if the through-bond interactions are predominated.[51] Recently, the intramolecular through-space and through-bond ($n_N \leftrightarrow n_N$ or $\pi_{CC} \leftrightarrow \pi_{CC}$) interactions in 1,4-diazabicyclo[2,2,2]-octane, 1,4-cyclohexadiene, and 2,5-norbornadiene were investigated with the 2D-PIES technique.[55] If the conclusion for the identical lone pairs is extended to the unequivalent lone pairs of this work, we also can identify the mechanism of the interactions. In Figures 4 and 5, the a″-type orbitals have the out-of-plane electron distributions, and the a′-type orbitals have the in-plane electron distributions. If one focuses on the characteristics of electron distributions on the Cl and I atoms, the symmetrical overlap between the I and Cl distribution regions can be found in the map of 27a′ (high energy level), but no overlap can be found in the map of 26a′ (low energy level) in Figure 5. It suggests that the intramolecular though-bond (σ_{CI} bond) interactions are predominated for these two orbitals. However, the characteristics of $n_I^{||}$ for 28a′ and σ_{CCl} for 25a′ are predominated, both the through-space and through-bond interactions may be involved and the interactions are relatively weak because of the larger energy separation between these two orbitals. It is much clearer for the cases of CH_2ClCN in Figure 6. The overlap between the $n_{Cl}^{\perp}$ and $\pi_{CN}^{\perp}$ is observed in the map of 4a″ (high energy level) rather than 3a″ (low energy level), which indicates that $n_{Cl}^{\perp} \leftrightarrow \pi_{CN}^{\perp}$ interactions are of the through-bond (σ_{CH}). The remarkable overlap between $n_{Cl}^{||}$ and $\pi_{CN}^{||}$ is observed in the map of 14a′ (low energy level) rather than 15a′ (high energy level), which indicates that the through-space $n_{Cl}^{||} \leftrightarrow \pi_{CN}^{||}$ interactions occur. On the other hand, the characteristics of Cooper minima for the halogen n orbitals have been studied with the angle-resolved photoelectron spectra of dihalomethanes.[32] The authors found that the angular distribution parameter β spectra of the lone pair orbital of CH_2ClI showed strong evidence of mixed halogen character but no evidence for CH_2BrCl.[32] The stronger intramolecular orbital interactions result in the delocalized (mixed) MO characteristics, further being reflected by the different CEDPICS for respective band and interaction potentials. In Figure 7, the calculated potential energy curves indicate that the position of minima is at $\theta \sim 80°$ for the I atom, $\sim 85°$ for the Cl atom in CH_2ClI, and $\sim 105°$ for the Cl atom in CH_2ClCN.

D. CEDPICS and Anisotropic Interactions. In Figures 3 and 4, the CERPIES are helpful to recognize the MO characteristic of each band. In particular, the decreases of cross sections for bands S and S* differ from those for the neighboring bands in Figure 3. The atomic structures of band S* are clearer in the cold spectrum than those in the hot spectrum. CEDPICS for these bands obtained from the normalized CERPIES has been shown in Figures 5 and 6. It is contrast to the spin−orbit split bands that bands 1, 2, 3, and 4 for these two molecules show significantly different slopes of CEDPICS as given in Tables 1 and 2. For CH_2ClI, the slope parameter ($m = -0.41$) of band 1 is more negative than that ($m = -0.35$) of band 2. This can be explained by two facts: in Figure 5, the density map of 28a′ orbital shows some σ_{CCl} character, and the approach along the CCl bond axis (the E direction in Figure 8b) is repulsive, whereas the in-plane approaches (corresponding to the in-plane branch $n_I^{||}$) perpendicular to the CI bond axis (the L and M directions in Figure 8c) are attractive. However, the electrons of 11a″ orbital are mostly localized on the I atom as the out-of-plane (perpendicular to the molecular nodal plane) branch ($n_I^{\perp}$) in Figure 5, and the perpendicular approach (the K direction in Figure 8c) is remarkably attractive by exhibiting a well depth of ca. 350 meV larger than that for the in-plane perpendicular approach (ca. 170 meV in the L direction or ca. 80 meV in the M direction). Correspondingly, the slopes of CEDPICS for the bands (1, 4, and 7) having the out-of-plane electron distributions are more negative than those for the bands (2, 3, 5, and 6) having the in-plane characteristics. In particular, band 4 (mainly having the $n_{Cl}^{\perp}$ characteristic) exhibits the almost equal slope parameter compared with that of band 1. This may be interpreted by such process that the out-of-plane He* trajectories pointing to the Cl atom could be changed to the I atom because the out-of-plane approach to the I atom (the K direction) is much more attractive than that to the Cl atom (with a reference of the O direction) in Figure 8c and the smaller part of the density map of 10a″ (see Figure 5) covers the I position. Band 7 having the π_{CH} characteristic shows a larger negative slope ($m = -0.34$) for CH_2ClI with respect to that of the corresponding band for CH_2ClCN ($m = -0.08$). Similarly, this can be explained by the above discussions and the fact that the most attractive interaction is the head-on approach to the N atom in CH_2ClCN (see the potential curve in the direction A of Figure 8a). A little more attractive approach for band 7 leads to the higher band density in the PIES of CH_2ClI (see Figure 1) with respect to that in the PIES of CH_2ClCN (see Figure 2). Moreover, bands S and 2 show the comparable slope, but band S cannot be the satellite state related to band 2 ($28a'^{-1}$) because of the large pole strength of the second ionic state (0.95 of $28a'^{-1}$). The absolute slope value of CEDPICS for band S* is the smallest among the bands observed for CH_2ClI, which indicates either weak attractive or repulsive potential character around the avoided crossing between He^*-CH_2ClI and $He-CH_2ClI^{**}$ potential energy surfaces.

For CH_2ClCN, the MO electron density distributions and the slopes of CEDPICS are more complex than those for CH_2ClI and CH_2BrCN,[31] because of the stronger orbital $n_{Cl} \leftrightarrow \pi_{CN}$ interactions in CH_2ClCN. At first, one may notice the distinctly different slopes for bands 5 and 7. The former (13a′ having the n_N character) corresponds to the most attractive interaction which is exhibited by the calculated potential curve (the direction A) in Figure 8a. The curve for the direction A shows a large well depth ca. 300 meV, and the ΔE of band 5 correspondingly is the largest negative value (-200 ± 10 meV) among the observed peak shifts of all of the bands for CH_2ClCN in Table 2. The latter (2a″ having the π_{CH} characteristic) corresponds to the repulsive interaction (the direction I in Figure 8b), and the much less negative or positive ΔE (40 ± 120 meV) has been observed. More details on the first four bands are given

subsequently. Unlike bands 1 and 2 for CH_2ClI, band 1 (4a″ having the out-of-plane electron distributions) shows a smaller negative slope of CEDPICS than band 2 (15a′ having the in-plane electron distributions). In Figure 6, the MO electron distributions of 4a″ can be divided into three parts, $n_{Cl}^{\perp}$, $\pi_{CN}^{\perp}$, and σ_{CH}, and those of 15a′ can be divided into two parts, $n_{Cl}^{\parallel}$ and $\pi_{CN}^{\parallel}$. In Figure 8, parts a and b, the access in the direction F (corresponding to $n_{Cl}^{\perp}$) shows a shallow potential well (with a depth ca. 100 meV), whereas the access in the direction B (corresponding to $\pi_{CN}^{\perp}$) is repulsive. Thereby, the compositions of $\pi_{CN}^{\perp}$ and σ_{CH} result in the weaker collision energy dependence of band 1 with respect to band 2. Similarly, the composition σ_{CH} of 14a′ leads to a less negative slope with respect to that of band 4 (3a″).

Moreover, some arguments on the interaction differences between the CN group and halogen atoms are addressed. The CN group is usually called as pseudo halogen atom, but the different anisotropy of interactions between the CN group and halogen atoms with the He* atoms is found in this work. For the most cases, the head-on approach to the N atom in the CN group is much more attractive than the approaches in the other directions because the n_N electrons are mostly distributed along the CN bond axis.[27,31] The halogen n_X electron distribution are perpendicular to the CX bond axis, interpreting the more attractive approaches in the perpendicular directions with respect to the head-on approach to the halogen atom.[29−31] However, the collinear approach to the F atom in CF bond shows a little more attractive because of the much small van der Waals radius of F atom.[56] In this work, the distinguished anisotropic interactions are found around the I atom in CH_2ClI, in particular, the significantly attractive interaction is for the out-of-plane access (see Figure 8c). It may be interpreted by the intramolecular orbital interactions: the strong in-plane (a′-type) orbitals interact much more strongly than the out-of-plane (a″-type) orbitals, and the former makes the n_I electrons to be delocalized to the other parts where the in-plane approaches are less attractive (even strongly repulsive for the collinear approach to the CCl bond and the approach to the CH_2 group).

V. Conclusion

The PIES of CH_2ClI and CH_2ClCN by collision with the metastable He*(2^3S) atoms have been measured. The separated bands at the low ionization energy region are mainly arising from the intramolecular orbital interactions rather than the spin−orbit coupling effects. In the PIES of CH_2ClI, an additional band labeled with S may be related to autoionizations of the superexcited states of CH_2ClI, whereas the other band labeled with S* is proposed to be related to autoionizations of Rydberg state Cl** or I** species produced by the excitation transfer to CH_2ClI followed with the molecular dissociations. The through-space and through-bond interactions are proposed in these two molecules. The calculations of the magnitudes of the orbital interactions show the $n_{Cl} \leftrightarrow \pi_{CN}$ interactions are much stronger than $n_{Cl} \leftrightarrow n_I$, with the references of experimental spectra in this work and available in the literatures.[32−34,37,51] Furthermore, the strong intramolecular orbital interactions in these two molecules lead to the distinctly different slopes of CEDPICS for the first four bands (related to the lone pair orbitals of the Cl and I atom and the π_{CN} orbitals).

Acknowledgment. This work is partially supported by a Grant in Aid for Scientific Research from the Japanese Ministry of Education, Science and Culture. One of the authors (S.X.T.) thanks the Japan Society for the Promotion of Science (JSPS) for a JSPS postdoctoral fellowship (ID No.00111).

References and Notes

(1) Penning, F. M. *Naturwissenshaften* **1927**, *15*, 818.
(2) Illenberger, E.; Niehaus, A. *Z. Phys. B* **1975**, *20*, 33
(3) Parr, T. P.; Parr, D. M.; Martin, R. M. *J. Chem. Phys.* **1982**, *76*, 316.
(4) Allison, W.; Muschlitz, E. E., Jr. *J. Electron Spectrosc. Relat. Phenom.* **1981**, *23*, 339.
(5) Riola, J. P.; Howard, J. S.; Rundel, R. D.; Stebbings, R. F. *J. Phys. B* **1974**, *7*, 376.
(6) Woodard, M. R.; Sharp, R. C.; Seely, M.; Muschlitz, E. E., Jr. *J. Chem. Phys.* **1978**, *69*, 2978.
(7) Appolloni, L.; Brunetti, B.; Hermanussen, J.; Vecchiocattivi, F.; Volpi, G. G. *J. Chem. Phys.* **1987**, *87*, 3804.
(8) Lindinger, W.; Schmeltekopf, A. L.; Fehsenfeld, F. C. *J. Chem. Phys.* **1974**, *61*, 2890.
(9) Pesnelle, A.; Watel, G.; Manus, C. *J. Chem. Phys.* **1975**, *62*, 3590.
(10) Niehaus, A. *Adv. Chem. Phys.* **1981**, *45*, 399.
(11) Hotop, H.; Niehaus, A. *Z. Phys.* **1969**, *228*, 68.
(12) Ohno, K.; Mutoh, H.; Harada, Y. *J. Am. Chem. Soc.* **1983**, *105*, 4555.
(13) Yencha, A. J. In *Electron Spectroscopy: Theory, Technique and Application*; Brundle, C. R., Baker, A. D., Eds.; Academic: New York, 1984; Vol. 5.
(14) Benz, A.; Leisin, O.; Morgner, H.; Seiberle, H.; Stegmaier, J. *Z. Phys. A* **1985**, *320*, 11.
(15) Tian, S. X.; Kishimoto, N.; Ohno, K. *Chem. Phys. Lett.* **2002**, *365*, 40.
(16) Beckmann, K.; Leisin, O.; Morgner, H. *Mol. Phys.* **1986**, *59*, 829.
(17) Čermák, V. *J. Chem. Phys.* **1966**, *44*, 3781.
(18) Mitsuke, K.; Takami, T.; Ohno, K. *J. Chem. Phys.* **1989**, *91*, 1618.
(19) Ohno, K.; Takami, T.; Mitsuke, K.; Ishida, T. *J. Chem. Phys.***1991**, *94*, 2675.
(20) Takami, T.; Mitsuke, K.; Ohno, K. *J. Chem. Phys.* **1991**, *95*, 918.
(21) Dunlavy, D. C.; Martin, D. W.; Siska, P. E. *J. Chem. Phys.* **1990**, *93*, 5347.
(22) Longley, E. J.; Dunlavy, D. C.; Falcetta, M. F.; Bevsek, H. M.; Siska, P. E. *J. Phys. Chem.* **1993**, *97*, 2097.
(23) Siska, P. E. *Rev. Mod. Phys.* **1993**, *65*, 337.
(24) Ohno, K.; Yamakado, H.; Ogawa, T.; Yamata, T. *J. Chem. Phys.* **1996**, *105*, 7536.
(25) Hotop, H. *Radiat. Res.* **1974**, *59*, 379.
(26) Auerbach, D. J. In *Atomic and Molecular Beam Methods*; Scoles, G., Eds.; Oxford University Press: New York, 1988; p 369.
(27) Kishimoto, N.; Aizawa, J.; Yamakado, H.; Ohno, K. *J. Phys. Chem. A* **1997**, *101*, 5038.
(28) Niehaus, A. *Ber. Bunsen-Ges. Phys. Chem.* **1973**, *77*, 632.
(29) Tian, S. X.; Kishimoto, N.; Ohno, K. *J. Phys. Chem. A* **2002**, *106*, 6541.
(30) Tian, S. X.; Kishimoto, N.; Ohno, K. *J. Electron Spectrosc. Relat. Phenom.* **2002**, *125*, 205.
(31) Tian, S. X.; Kishimoto, N.; Ohno, K. Submitted.
(32) Novak, I.; Benson, J. M.; Potts, A. W. *Chem. Phys.* **1986**, *107*, 129.
(33) Novak, I.; Cvita, T.; Klasinc, L.; Güsten, H. *J. Chem. Soc., Faraday Trans. 2* **1981**, *77*, 2049.
(34) Novak, I.; Li, D. B.; Potts, A. W.; Shareef, A.; Kovac, B. *J. Org. Chem.* **2002**, *106*, 2850.
(35) Zerefos, C. S.; Isaken, I. S. A.; Ziomas, I. *Chemistry and Radiation Changes in the Ozone Layer*; Kluwer: Dordrecht, The Netherlands, 2001.
(36) Gardner, J. L.; Samson, J. A. R. *J. Electron Spectrosc. Relat. Phenom.* **1976**, *8*, 469.
(37) Kimura, K.; Katsumata, S.; Achiba, Y.; Yamazaki, T.; Iwata, S. *Handbook of He I Photoelectron Spectra of Fundamental Organic Molecules*; Japan Scientific: Tokyo, 1981; and references therein.
(38) Turner, D. W.; Baker, C.; Baker, A. D.; Brundle, C. R. *Molecular Photoelectron Spectroscopy*; Wiley: London, 1970.
(39) (a) Yee, D. S. C.; Stewart, W. B.; Mcdowell, C. A.; Brion, C. E. *J. Electron Spectrosc. Relat. Phenom.* **1975**, *7*, 93. (b) Hotop, H.; Hükler, G. *J. Electron Spectrosc. Relat. Phenom.* **1977**, *11*, 101.
(40) Stevens, W.; Basch, H.; Krauss, J. *J. Chem. Phys.* **1984**, *81*, 6026.
(41) Pauling, L. *The Nature of the Chemical Bond*; Cornell University: Ithaca, New York, 1960.
(42) (a) von Niessen, W.; Schirmer, J.; Cederbaum, L. S.; *Comput. Phys. Rep.* **1984**, *1*, 57. (b) Zakrzewski, V. G.; Ortiz, J. V. *Int. J. Quantum Chem. Symp.* **1994**, *28*, 23. (c) Zakrzewski, V. G.; Ortiz, J. V. *Int. J. Quantum Chem.* **1995**, *53*, 583.
(43) Rothe, E. W.; Neynaber, R. H.; Trujillo, S. M. *J. Chem. Phys.* **1965**, *42*, 3310.

(44) Haberland, H.; Lee, Y. T.; Siska, P. E. *Adv. Chem. Phys.* **1981**, *45*, 487.

(45) Hotop, H.; Roth, T. E.; Ruf, M.-W.; Yencha, A. J. *Theor. Chem. Acc.* **1998**, *100*, 36.

(46) Frisch, M. J.; Trucks, G. W.; Schlegel, H. B.; Scuseria, G. E.; Robb, M. A.; Cheeseman, J. R.; Zakrzewski, V. G.; Montgomery, J. A., Jr.; Stratmann, R. E.; Burant, J. C.; Dapprich, S.; Millam, J. M.; Daniels, A. D.; Kudin, K. N.; Strain, M. C.; Farkas, O.; Tomasi, J.; Barone, V.; Cossi, M.; Cammi, R.; Mennucci, B.; Pomelli, C.; Adamo, C.; Clifford, S.; Ochterski, J.; Petersson, G. A.; Ayala, P. Y.; Cui, Q.; Morokuma, K.; Malick, D. K.; Rabuck, A. D.; Raghavachari, K.; Foresman, J. B.; Cioslowski, J.; Ortiz, J. V.; Stefanov, B. B.; Liu, G.; Liashenko, A.; Piskorz, P.; Komaromi, I.; Gomperts, R.; Martin, R. L.; Fox, D. J.; Keith, T.; Al-Laham, M. A.; Peng, C. Y.; Nanayakkara, A.; Gonzalez, C.; Challacombe, M.; Gill, P. M. W.; Johnson, B. G.; Chen, W.; Wong, M. W.; Andres, J. L.; Head-Gordon, M.; Replogle, E. S.; Pople, J. A. *Gaussian 98*; Gaussian, Inc.: Pittsburgh, PA, 1998.

(47) (a) Various saturated halocarbons have been studied by Ohno et al. (unpublished work) in comparisons between He I UPS and He*(2^3S) PIES. For the larger halocarbons, the spin−orbit split bands show different shapes in a same spectrum (UPS or PIES), and the higher-electron-energy band is a little stronger than the other in the PIES. (b) Recently, the 2D-PIES of CH_3I has been studied in our group. The slope parameters m of CEDPICS for the SO split bands of the n_I orbital are almost equal ($m = -0.42 \pm 0.02$; -0.42 ± 0.01).

(48) (a) Yencha, A. J.; Ganz, J.; Ruf, M.-W.; Hotop, H. *Z. Phys. D* **1989**, *14*, 57. (b) Imura, K.; Kishimoto, N.; Ohno, K. *J. Phys. Chem. A* **2002**, *106*, 3759.

(49) Lescop, B.; Ben Arfa, M.; Cherid, M.; Le Coz, G.; Sinou, G.; Le Nadan, A.; Tuffin, F. *J. Phys. B* **1997**, *30*, 1241.

(50) Only a part of band 8 appears in the PIES of Figures 1 and 3 because of the energy limitation of the He* atom (19.82 eV). CEDPICS of band 8 (not shown in Figure 5) exhibits a slope ($m = -0.23$), and the density map of 24a′ shows the characteristics of C_{2s} orbital. The flatter slope with respect to the others also indicates occurrence of the Auger-like autoionization (see the discussions in ref 20).

(51) Eland, J. H. D. *Photoelectron Spectroscopy: An introduction to ultraviolet photoelectron spectroscopy in the gas phase*; Butterworth: London, 1974; and references therein.

(52) Rabalais, J. W. *Principles of Ultraviolet Photoelectron Spectra*; John Wiley & Sons: New York, 1977.

(53) (a) Hoffmann, R.; Imamura, A.; Hehre, W. J. *J. Am. Chem. Soc.* **1968**, *90*, 1499. (b) Hoffmann, R. *Acc. Chem. Res.* **1971**, *4*, 1.

(54) Heilbronner, E.; Maier, J. P. In *Electron Spectroscopy: Theory, techniques and Applications*; Brundle, C. R., Baker, A. D., Eds.; Academic Press: New York, 1977; Vol. 1.

(55) Kishimoto, N.; Ogasawara, H.; Ohno, K. *Bull. Chem. Soc. Jpn.* **2002**, *75*, 1503.

(56) Imura, K.; Kishimoto, N.; Ohno, K. *J. Phys. Chem. A* **2001**, *105*, 6378.